Journal of Membrane Science 548 (2018) 22–31

Contents lists available at ScienceDirect

Journal of Membrane Science

journal homepage: www.elsevier.com/locate/memsci

On negative rejection of uncharged organic solutes in forward osmosis

Arnout K.H. D'Haese[a,*], Ilse De Leersnyder[b], Pieter Vermeir[b], Arne R.D. Verliefde[a]

[a] Particle and Interfacial Technology group (PaInT), Department of Applied Analytical and Physical Chemistry, Faculty of Bioscience Engineering, Ghent University, Coupure Links 653, B-9000 Ghent, Belgium

[b] Laboratory of Chemical Analysis (LCA), Department of Applied Biosciences, Faculty of Bioscience Engineering, Ghent University, Valentyn Vaerwyckweg 1, Schoonmeersen, B-9000 Ghent, Belgium

ARTICLE INFO

Keywords:
Forward osmosis
Negative rejection
Organic solutes
Transport modeling

ABSTRACT

Negative rejection of 7 alcohols in Forward Osmosis (FO) is reported. The alcohols used in this study are uncharged, hydrophilic organic solutes. It is shown that current membrane transport models are not capable of reproducing the rejection pattern presented here, and consequently, a new model is developed. The model relies on adsorption of the solutes to the membrane followed by coupled transport. Adsorption is caused by salting out of the solutes, while coupled transport is caused by their small size and hydrophilicity, yielding comparatively strong water-solute interactions. It is calculated that the solutes are enriched 4–5 times in the membrane compared to the feed solution. Coupled transport is also demonstrated using the same membrane and solutes in RO mode. The novel model yields an excellent fit, and model parameters are discussed.

1. Introduction

Negative rejection of feed solutes by membranes, i.e. enrichment of a feed solute in permeate, is a relatively rare phenomenon. In this study, negative rejection of organic, uncharged solutes during forward osmosis (FO) is described and modeled, with the solutes being 7 alcohols. Negative rejection in aqueous solutions is rarely encountered because of some properties of water. Compared to organic solutes, water has a small molar volume, high diffusivity, is strongly polar and has a high surface tension. High diffusivity and high surface tension of water both contribute to high feed solute rejection: water diffusion across a membrane active layer is relatively fast compared to feed solutes, and the high surface tension causes strong solute-water and water-membrane interactions, diminishing the importance of solute-membrane interactions [1,2]. The contribution of a low molar volume to rejection is more ambiguous. Small molecules are less sterically hindered during membrane permeation, but on the other hand, the chemical activity of a solute in a pressurized incompressible fluid increases exponentially with molar volume [3,4,2], the latter causing increasing diffusivity at increasing pressure, coined pressure-induced diffusion.

Much of the research into negative rejection has focused on organic solvent nanofiltration (OSN), as negative rejection is encountered more frequently in non-aqueous solutions [1,2,5–7]. In OSN, solvent surface tension is much lower compared to water, allowing for stronger solute-membrane interactions. Negative rejection is reported for solutes having a high solute-membrane affinity [1,6,7], and stronger negative rejection for solutes of increasing size has been reported as well. For instance, the latter has been observed by Postel et al. [6] for homologue series of alkanes, styrene and ethylene glycol oligomers. This seemingly contradictory result can be explained by the exponential increase of solute chemical activity due to increased molar volume and thus increased flux [3,2], and can be modeled using a generalized solution-diffusion model [2,7].

In aqueous solutions, negative rejection has been observed mainly for ionic solutes. In nanofiltration, negative rejection of ions has been studied in depth by Yaroshchuk [8] who defined different mechanisms which can cause negative rejection. Such mechanisms are Donnan potential decreasing the rejection of mobile counterions, enrichment of ions in the membrane phase of charged membranes (particularly charge-mosaic membranes), or the acceleration of ions in the membrane phase. Perry and Linder [9] presented a modified Spiegler-Kedem model including a Donnan exclusion correction which could describe negative ion rejection. Negative rejection of uncharged organic solutes in aqueous solutions has been observed, a well-described case being phenolic compounds permeating through cellulose acetate (CA) RO membranes [10–12]. It was noted that rejection became more negative with increasing pressure, and negative rejection was explained as a combination of strong adsorption of phenolic compounds on CA and an increase of their chemical potential due to the exerted pressure, similar to the generalized solution-diffusion model. Mandale and Jones [13] observed negative rejection of 5 uncharged, non-dissociable organic compounds in the presence of Na_2HPO_4 during NF. The results were

* Corresponding author.
E-mail address: arnout.dhaese@ugent.be (A.K.H. D'Haese).

http://dx.doi.org/10.1016/j.memsci.2017.11.002
Received 1 May 2017; Received in revised form 23 October 2017; Accepted 1 November 2017

interpreted using the model presented by Perry and Linder; assuming that the organic compounds were in fact partially charged. This assumption appears questionable: the organics, 3 sugars, an alcohol and caffeine, were required to substitute for Na^+ ions according to the Donnan model, even though all of those compounds are Lewis bases [14] and hold no permanent charges.

In this study, negative rejection of uncharged organic solutes during FO is reported, in the absence of a transmembrane hydraulic pressure difference. The rejection pattern presented in this study shows strong negative rejection at low water flux, and rejection increases and becomes positive as the water flux increases. As is shown below, commonly used transport models are however unable to reproduce this rejection pattern, or are unable to predict negative rejection altogether. Therefore, in order to describe this phenomenon, a new transport model is needed. Compared to the above described cases, the driving forces and feed solute chemical activity in FO are different. Given the absence of a transmembrane pressure difference, feed solute flux is not subject to pressure-induced diffusion, and feed solute activity is only modulated by feed solute-draw solute interactions. The latter interactions can lead to salting-in or salting-out, in which the solute chemical activity is reduced or increased respectively [15]. Salting effects are explored by comparing solute rejection during both FO and RO, using the same membrane and at similar water fluxes, yielding contrasting rejection patterns. A new mechanistic model is developed, based on sequential adsorption followed by washing out of the adsorbed solutes by the water flux; the latter process assumes flux coupling between water and the feed solutes. Differences between FO and RO results are discussed, and flux coupling as well as salting effects are explored.

2. Materials and methods

2.1. Chemicals and analysis

The non-ionic organics used in this study were 7 alcohols (Sigma-Aldrich), the properties of which are given in Table 1. N_aCl was used as a draw solute, draw solution concentrations ranged from 0.15 to 5.3 M. The alcohols were used at a concentration of 100 mg/L each, and were used as a mixture. As the alcohols dissolved in the feed and draw solutions were quantified by headspace-GC-MS, the influence of salting effects by N_aCl on alcohol volatility cannot be neglected. To this end, isobutanol was added to all samples as an internal standard. In order to account for quantitatively different salting effects for the different alcohols, volatility of each alcohol relative to isobutanol as a function of N_aCl concentration was quantified in a N_aCl dilution series. The dilution series consisted of 8 alcohol standards in N_aCl solutions spanning 0–5 M N_aCl; the relative deviation compared to the isobutanol response was measured. Salting out of alcohols was observed, which is qualitatively illustrated in Fig. 1, in which the GC-MS detector response for the N_aCl dilution series is plotted for each alcohol Table 2. It should be noted that the alcohol concentration was the same in each sample of the dilution series; the trend in GC-MS response is due to increased alcohol volatility. Also, at 5 M N_aCl, volatiliy of the analytes relative to isobutanol was in the range of 75–135% compared to pure water, clearly showing that volatility deviations could not be ignored.

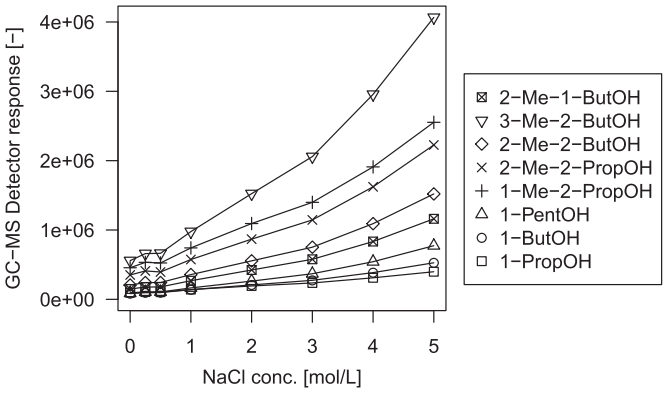

Fig. 1. GC-MS detector response for each alcohol as a function of NaCl concentration, showing salting out of the alcohols. Alcohol concentration was equal in all samples.

Samples were analyzed using Headspace GC-MS, using an Agilent 6890 GC equiped with a Gerstel MPS headspace injection system. The sample vials were incubated at 80 °C during 5 min while shaking prior to sampling. The syringe temperature was maintained at 90 °C. The injection volume was 2500 µl. The inlet temperature was set at 230 °C. A split ratio of 50:1 was used; using helium as carrier gas. The GC was equiped with an Alltech Hiliflex 15,881 column of 30 m length and 0.25 µm film thickness. The GC oven temperature was ramped from 35 °C to 200 °C, using an initial ramp rate of 3°/min for 10 min followed by 20°/min for the remaining 6.75 min runtime. The MS detector was an Agilent 5973 mass selective detector.

Table 1
Properties of the feed solutes used in this study. References for diffusivity: [a] Hoa and Leaist [16], [b] Funazukuri [17]; density: vendor MSDS, Pubchem, ChemSpider.

Name	Molecular str.	Density (kg/m^3)	Diffusivity (10^{-9} m^2/s)	Abbreviation
1-propanol	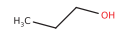	803	1.06[a]	1-PropOH
1-butanol	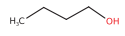	810	0.96[a]	1-ButOH
2-methyl-2-propanol	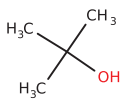	781	0.88[a]	2-Me-2-PropOH
1-pentanol	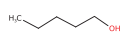	811	0.89[a]	1-PentOH
2-methyl-1-butanol	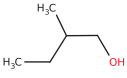	815	0.92[b]	2-Me-1-ButOH
2-methyl-2-butanol	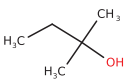	815	0.87[b]	2-Me-2-ButOH
3-methyl-2-butanol	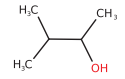	818	0.90[b]	3-Me-2-ButOH

Table 2
Fitted parameters for the *CDL* model.

CDL parameters	Value	Units
K_c	4.21–4.98	–
k_a^*	0.41–3.26	10^{-6} mol/(m^2 s)
S	10.7–32.0	10^{-3} m

2.2. FO setup and test protocols

The membranes used in this study, were cellulose triacetate membranes with embedded support (CTA) (HTI, USA). The membranes were stored suspended in deionized water and refrigerated at 4 °C. A scheme of the FO setup is given in Fig. 2. The setup was airtight, in order to limit the loss of the volatile alcohols. The feed and draw reservoirs were Schott bottles which were closed off with an open cap and rubber septum. Through the septum, solution inlet and outlet ports, a sampling port and a connection to a gas bag were fitted. The gas bag was added to accommodate the volume change inside the feed and draw reservoirs during FO; the gas bag of the feed solution was partially inflated with N_2 at the beginning of each test. Mass balances were calculated for all FO tests, yielding alcohol recoveries of 98.8 ± 3.1%, showing negligible loss of solutes over the course of the experiments. A variable-speed peristaltic pump (Cole-Parmer) and food-grade Norprene tubing were used, the total length of the latter was kept to an absolute minimum to limit alcohol losses due to adsorption or volatilization. This yielded a volume of about 50 ml for each compartment. The effective membrane surface area was 124.14 cm^2, with the flow channels being 50 mm wide, 250 mm long and 1 mm high. A diamond-type RO feed spacer was fitted in both compartments to counteract external concentration polarization. Cross flow was set at 0.15 m/s, resulting in an ECP modulus of at most 1.14 for the highest water flux. The weight of the feed solution was logged using an OHaus Pioneer 4201 scale (OHaus, USA) and a LabVIEW (NI, USA) script.

Prior to the FO tests, feed solution was recirculated in the feed compartment during 24 h in order to saturate the tubing with the alcohols. In between FO tests, both compartments were rinsed using 250 ml deionized water in a once-through fashion which was pumped through slowly, after which the draw solution compartment was similarly rinsed with 100 ml draw solution to remove any remaining deionized water. The feed and draw solution volume were 500 and 200 ml respectively, fresh batches of feed and draw solution were prepared for each experiment. The feed and draw volumes were selected based on analytical considerations: a larger feed solution volume compared to the draw solution allows for a more stable feed solution composition during FO tests, while the small draw solution volume limits error propagation during rejection calculation. Experiments were stopped after the production of 100 ml permeate, implying that 33% of the final draw solution volume was permeate. 8 FO tests at different fluxes were performed, with fluxes ranging from 0.6 to 6.0 µm/s. Average J_w was calculated, with A_m and t being the membrane surface area time elapsed respectively, according to the following mass balance:

$$J_w = \frac{\Delta V}{A_m \Delta t} \tag{1}$$

The feed solution was sampled at the start and end of each experiment, the draw solution was sampled at the end. Samples of 10 ml were taken without opening feed or draw solution containers and were stored in 12 ml sample size Exetainer sampling vials (Labco, UK) fitted with rubber septa. Sample vials were stored refrigerated and were never opened in order to limit volatile losses. External concentration polarization (ECP) was calculated according to film theory [18], using Eq. (2) for poorly rejected solutes:

$$\frac{c_m}{c_f} = \frac{c_p}{c_f}\left[1 - exp\left(\frac{J_w}{k}\right)\right] + exp\left(\frac{J_w}{k}\right) \tag{2}$$

To calculate k, Eq. (3) was used [19,20]:

$$Sh = 0.2Re^{0.57}\,Sc^{0.4} = \frac{d_h k}{D} \tag{3}$$

with d_h and D being the module hydrodynamic diameter and the solute diffusivity. Rejection is calculated as:

$$R = 1 - \frac{c_p}{c_m} \tag{4}$$

2.3. RO setup and test protocols

The RO setup consisted of a Sterlitech HP4750 stirred cell having a membrane surface area of 12.0 cm^2 fitted with a PTFE stirrer bar to provide cross flow. This cell has a low hold-up volume of 1 ml and a feed volume of 300 ml. Membrane coupons were compacted at 30 bars until constant flux, which lasted 2 h. RO tests were performed at 5, 10, 14, 20, 25 and 30 bars. Permeate was collected in glass-only gas sampling syringes in order to avoid solute volatilization. The first 5 ml of permeate were discarded, after which 10 ml was collected. The syringe was placed on a OHaus Adventurer Pro 410 scale which was datalogged for flux measurements. The feed solution was used for 3 RO tests, after which it was discarded and fresh feed solution was prepared. The stirrer was set to 250 rpm, which corresponded to a stirrer tip velocity of 0.26 m/s. Sample handling and storage was as described in the previous section. The external concentration polarization mass transfer coefficient k was calculated according to [21]:

$$k = 0.23\frac{D}{r}\left(\frac{\nu}{D}\right)^{1/3}\left(\frac{\omega r^2}{\nu}\right)^{0.567} \tag{5}$$

with ν, D, ω and r being the kinematic viscosity, solute diffusion coefficient, angular velocity and stirrer radius. This then allowed the calculation of the real rejection, with R_{obs} being the observed rejection, according to [21]:

$$R = \frac{R_{obs}exp\left(\frac{J_w}{k}\right)}{(1 - R_{obs}) + R_{obs}exp\left(\frac{J_w}{k}\right)} \tag{6}$$

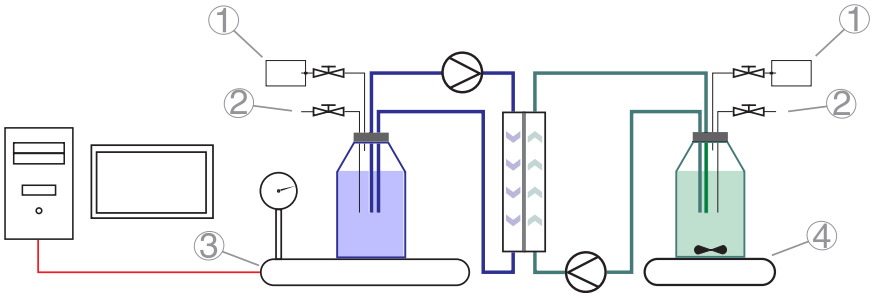

Fig. 2. Scheme of the gas-tight FO setup. The feed and draw reservoirs were closed using rubber septa, through which ports were fitted. In order to accommodate the volume changes of both solutions, gas sampling bags were included (1), with the feed gas sampling bag being partially inflated at the start of the test. Liquid samples were taken using long needles which were closed off with valves (2). The weight of the feed solution was logged (3), while the draw solution was stirred (4).

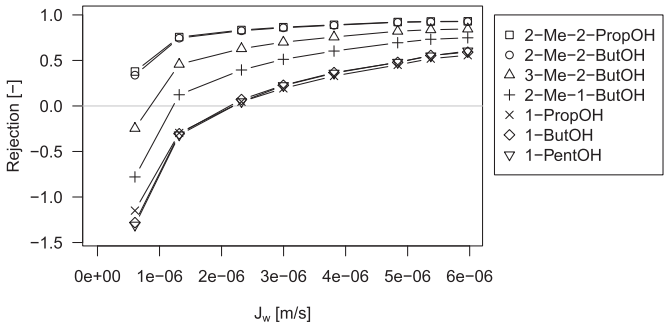

Fig. 3. Experimental FO rejection of the alcohols as a function of J_w. Data points joined by straight line segments for clarity, zero rejection indicated by gray line.

2.4. Modeling

All modeling was done in R 3.3.1 [22]. Parameter optimization was done using a modified, box-constrained Nelder-Mead simplex algorithm, minimizing the residual sum of squared errors between fitted and observed rejection.

3. Results: Observed rejection

3.1. FO rejection

The rejection of the alcohols as a function of water flux (J_w) is given in Fig. 3. Rejection increases as substitution of the alkyl chain increases, due to increasing steric hindrance. Rejection of all alcohols except the quaternary substituted 2-Me-2-PropOH and 2-Me-2-ButOH was negative at the lowest J_w and became positive as J_w increased. Straight chain alcohols (1-PropOH, 1-ButOH and 1-PentOH) show very similar rejection for all fluxes, clearly indicating that the solutes are oriented favorably during membrane transport: the length of the alkyl chain has a negligible influence on rejection, while the cross section perpendicular to the long axis of the alkyl chain is nearly identical for the 3 straight chain alcohols [23]. The rejection of the tertiary substituted alcohols (2-Me-1-ButOH and 3-Me-2-ButOH) is intermediary between the straight chain alcohols and the quaternary substituted, with the more constrained 3-Me-2-ButOH having a higher rejection than 2-Me-1-ButOH. For this series of alcohols, the solute-membrane interactions can be considered to be similar, given the relatively small variation in chain length. The variability of rejection within this series of solutes is then determined predominantly by steric hindrance.

3.2. RO rejection

The rejection of the alcohols as a function of J_w is given in Fig. 4. During FO and RO, J_w was very similar: water flux varied from less than 1 μm/s to 6 μm/s. Similarly to the rejection obtained during FO, rejection increases with alkyl chain substitution and increases with J_w.

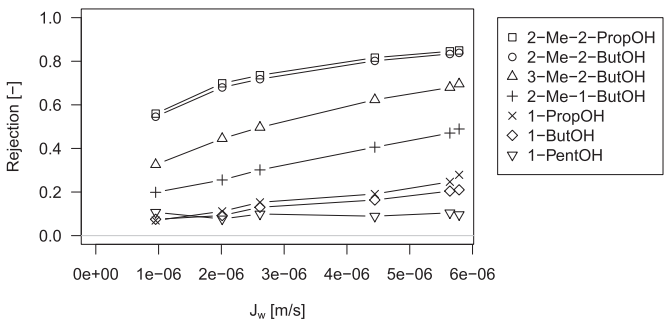

Fig. 4. Experimental RO rejection of the alcohols as a function of J_w. Data points joined by straight line segments for clarity, zero rejection indicated by gray line.

Using RO, rejection was positive at all times, although the rejection using FO at high J_w was higher than the rejection obtained using RO.

4. Membrane transport theory in the context of negative solute rejection

4.1. Existing models describing negative rejection

Dense membrane processes, such as FO or RO, are often modeled using the solution-diffusion (*SD*) model. Certain alternative versions of this model have been proposed, such as adsorption-solution-diffusion [24] or generalization of the *SD* model lacking simplifications regarding coupled diffusion, membrane affinity and the non-linear effect of pressure on solvent and solute transport [2]. Other popular models are the Spiegler-Kedem (*SK*) model [25] based on irreversible thermodynamics, and mechanistic models based on the extended Nernst-Planck equation [26]. For uncharged solutes, as is the case in this study, the extended Nernst-Planck reduces to a convection-diffusion model (*CD*), of which the coefficients can be interpreted using irreversible thermodynamics [25] or using binary Maxwell-Stefan coupled transport. The *SK* and *CD* models allow for coupled fluxes, in contrast with the classical *SD* model. It will be shown that the above mentioned models either cannot yield negative rejection patterns, or yield patterns different from the results presented in the above section. In order to explain the experimental results, clearly, current membrane transport theory needs to be extended.

In the classical *SD* model, J_s is proportional to the solute concentration difference across the membrane, with the membrane permeability coefficient B as the rate constant [3]:

$$J_s = B(c_f - c_p) \tag{7}$$

Given that $J_s = J_w c_p$ (neglecting ECP), this leads to the following expression for rejection:

$$R_{SD} = \frac{J_w}{B + J_w} \tag{8}$$

which, for a finite and positive B leads to the following limits:

$$\lim_{J_w \to 0} R_{SD} = 0 \quad \& \quad \lim_{J_w \to \infty} R_{SD} = 1$$

showing that solute rejection in the classical SD model is always positive. In Eq. (7), the solute concentration can be expressed using adsorption isotherms in the case of preferential solute adsorption [24]. However, the above formulated limits are still valid in the case of *SD-adsorption*, showing that negative rejection is again impossible.

In Eq. (7), which is based on Fick's law, ideal behavior of sufficiently dilute feed solutes is assumed. If this assumption would not be true, for instance due to vastly different feed and draw solution composition, rejection could become negative. Returning to the assumption in the *SD* model that flux is driven by continuous chemical potential gradients [3], the flux of a solute s can be written as:

$$J_s = -k_s c_s \frac{d\mu_s}{dx} \tag{9}$$

with k_s, c_s and x being a rate constant, solute concentration and 1D gradient coordinate respectively. During osmosis, under isobaric and isothermal conditions, the chemical potential of s (being uncharged) is given by:

$$\mu_s = \mu_0 + RTln(\gamma_s c_s) \tag{10}$$

Total differentiation of μ_s with respect to x leads to:

$$\frac{d\mu_s}{dx} = RT\left(\frac{1}{\gamma}\frac{d\gamma}{dx} + \frac{1}{c}\frac{dc}{dx}\right) \tag{11}$$

Which yields for J_s, with Eq. (11) integrated between the feed and permeate side, assuming linear gradients for γ and c:

$$J_s = \frac{k_s RT}{l} c_s ln\left(\frac{\gamma_f}{\gamma_p}\right) + \frac{k_s RT}{l}(_f - c_p) = Bc_s ln\left(\frac{\gamma_f}{\gamma_p}\right) + B(c_f - c_p) \quad (12)$$

It can be seen that when an activity coefficient gradient is absent ($\gamma_f = \gamma_p$), Eq. (12) reduces to the conventional expression of J_s (Eq. (7)). In Eq. (12), c_s is an average solute concentration, intermediate between c_f and c_p. Assuming $c_s = c_f$ implies that k_s is the rate constant at the feed-membrane interface. Using this assumption, rejection can be expressed analytically:

$$R = \frac{J_w - Bln\left(\frac{\gamma_f}{\gamma_p}\right)}{B + J_w} \quad (13)$$

If salting in occurs, $\gamma_f > \gamma_p$ is valid and accordingly, $-ln(\frac{\gamma_f}{\gamma_p}) < 0$. This yields for the limit at low J_w:

$$\lim_{J_w \to 0} R = -ln\left(\frac{\gamma_f}{\gamma_p}\right)$$

leading to negative rejection at low water flux. Although fitting Eq. (13) yields excellent agreement with experimental data (shown in Supplementary Information), strong salting in of the solute is assumed. This contradicts observations presented in Fig. 1, clearly showing salting out of the alcohols.

The generalized *SD* model, also referred to as coupled *SD* model, was developed to extend the *SD* model to organic separations, such as organic solvent nanofiltration (OSN), where effects of pressure on partial molar volume, solute-solvent flux coupling and solute- and solvent-membrane affinity become much more pronounced [2,7]. The effect of solute-solvent coupling of solutes with low membrane affinity in aqueous membrane separation was shown to be insignificant [2], although coupling cannot be neglected in the case of high solute-membrane affinity [7,1]. In the case of negligible flux coupling but retaining pressure-induced effects and sufficiently dilute feed solutions so that $\pi_f \approx 0$, solute rejection during pressure driven filtration is given by:

$$R = \frac{1 - exp(-y) - \alpha(1 - exp(-vy))}{1 - exp(-y) + \alpha exp(-vy)} \quad (14)$$

with y equaling $\frac{\overline{V}_p}{RT}$, the reduced pressure, α equaling the ratio of the solute and solvent membrane permeability and v equaling the ratio of solute to solvent partial molar volume. Negative rejection is possible in the generalized SD model due to two phenomena: firstly, hydrostatic pressure increases the activity of both solvent and solutes, with the effect being proportional to the exponential of the molar volume. A larger solute molar volume thus increases the solute's driving force to permeate through the membrane relative to the solvent. Secondly, the limiting rejection of this model at high flux is $R = 1 - \alpha$, which, when α is larger than unity, causes negative rejection [2]. However, rejection at the limit of $J_w \to 0$ equals 0, implying that negative rejection further decreases at increasing J_w, rather than becoming positive as was observed in this study. This is shown in Fig. 5. It should furthermore be pointed out that in FO, in the absence of hydrostatic pressure, feed solute activity is subject only to salting effects by the draw solute, not to pressure-induced effects.

Certain models allow for coupled fluxes, in contrast to the *SD* models discussed above. Such convection-diffusion models can be deduced from irreversible thermodynamics [25], Maxwell-Stefan theory [27] or reduced forms of the extended Nernst-Planck equation [26]. Convection-diffusion models consider the solute flux as the sum of a diffusive transmembrane flux and a solvent-coupled solute flux. Such models commonly consider viscous flow in which the solute is assumed to be entrained by the solvent during its passage through discrete membrane pores and are subjected to hindrance due to solute-pore wall collisions [26,28]. Flux coupling can also be considered on a molecular level rather than viscous flow; the former case is described by Maxwell-Stefan theory [29,30]. In its classical definition, the irreversible thermodynamics-based Spiegler-Kedem model allows for solute-solvent coupling by means of the reflection coefficient σ [25]. Feed solute flux is given by:

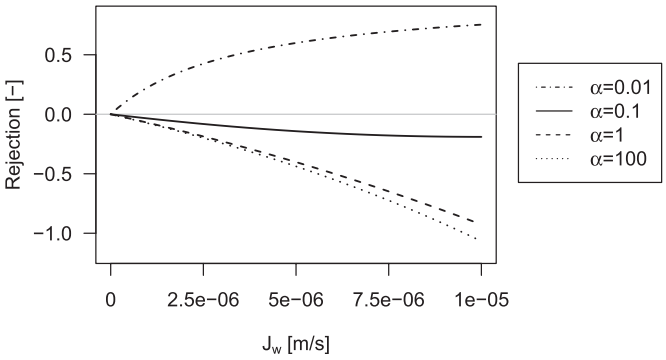

Fig. 5. Rejection according to the generalized solution-diffusion model of a solute with $r = 20$ as a function of J_w and α, the ratio of solute to solvent permeability. Reduced pressure ($\frac{\overline{V}_p}{RgT}$) was transformed into J_w assuming a hydraulic permeability of $2 \cdot 10^{-12}$m $\cdot$ Pa^{-1}s^{-1}.

$$J_s = \omega \Delta\pi + (1 - \sigma) J_v c \quad (15)$$

with $J_v \approx J_w$ for well-rejected solutes and σ defined as: $(\frac{\Delta p}{\Delta \pi})_{J_v = 0} = \sigma$, being the actual pressure applied to the feed at the point of zero flux to counteract feed osmotic pressure. It follows that for a perfect semi-permeable membrane, $\sigma = 1$, while a completely permeable membrane yields $\sigma = 0$. Rejection is given by:

$$R = \frac{(1 - F)\sigma}{1 - \sigma F} \quad with \quad F = exp(-\frac{J_v(1 - \sigma)}{B}) \quad (16)$$

Negative rejection is impossible however for finite and positive values of B and for $0 < \sigma < 1$, as is shown in the following limits:

$$\lim_{\sigma \to 0} R_{SK} = 0 \quad \& \quad \lim_{\sigma \to 1} R_{SK} = \frac{J_v}{J_v + B}$$

For $\sigma \to 1$, flux coupling is absent and Eq. (16) reduces to Eq. (8).

Describing feed solute flux using phenomenological coupled transport models, the hindrance factors K_c and K_d for convective and diffusive transport respectively are introduced [26]:

$$J_s = -D_\infty K_d \frac{dc}{dx} + K_c \frac{J_w}{\epsilon} c(x) \quad (17)$$

This model will be referred to as Convection-Diffusion (*CD*). Integration across the membrane active layer, taking into account solute partitioning ϕ, yields the following well-known expression for rejection:

$$R = 1 - \frac{\phi K_c}{1 - (1 - \phi K_c) exp\left(-\frac{J_w \phi K_c L}{\phi K_d D_\infty}\right)} \quad (18)$$

with $\frac{J_w \phi K_c L}{\phi K_d D_\infty} = Pe$, the Péclet number, and $L = \frac{l\tau^2}{\epsilon}$ being a structural parameter composed of the thickness l, porosity ϵ and tortuosity τ of the active layer [31]. K_c, K_d and ϕ are all dependent on λ, which is defined as: $\lambda = \frac{r_s}{r_p}$. Solutes are rejected completely if $\lambda > 1$ and are subjected to hindered transport when $0 < \lambda < 1$. Although different relations exist for the above 3 parameters as a function of λ, K_c and K_d are commonly considered polynomials with $K_c = K_d = 1$ for $\lambda = 0$ and $K_c = 1$, $K_d = 0$ for $\lambda = 1$ [28,32]. ϕ is dependent on pore shape and solute-membrane affinity: $\phi = (1 - \lambda)^2$ for cylindrical pores and $\phi = (1 - \lambda)$ for slit pores; solute membrane affinity can be incorporated as a Boltzmann distribution using the Gibbs free energy of interaction [33,34]:

$$\phi = (1 - \lambda)^z exp\left(-\frac{A_c \Delta G_i}{kT}\right) \quad with \quad z = 1, 2 \quad (19)$$

Since K_c is greater than unity for $0 < \lambda < 1$ and ϕ can be greater than

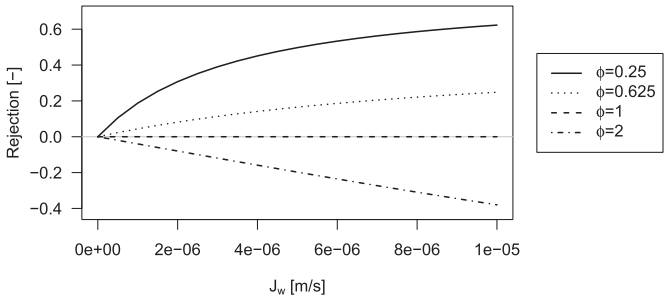

Fig. 6. Rejection according to the Convection-Diffusion model as a function of ϕ. Other parameters: $K_c = 1$, $K_d = 0.05$, $D_\infty = 1 \cdot 10^{-9}\,m^2\,s^{-1}$, $S = 4 \cdot 10^{-6}\,m$.

unity depending on the relative size and affinity of the solute, preferential solute transport is possible. K_c is considered greater than unity because it is reasoned that solutes which are larger than solvent molecules cannot approach the pore wall as closely as solvent molecules, and are thus found predominantly in the center of the pore where the solvent velocity is above average [28]. The limits of rejection as a function of J_w, however, show that a rejection pattern is obtained which is similar to the generalized *SD* case:

$$\lim_{J_w \to 0} R_{CD} = 0 \quad \& \quad \lim_{J_w \to \infty} R_{CD} = 1 - \phi K_c$$

For high ϕ, rejection at low J_w is close to 0 and decreases further with increasing J_w, as is shown in Fig. 6.

4.2. Novel model development

In the novel model, feed solute transport is assumed to be composed of two sequential processes: salting out causing adsorption of the solutes on the membrane material, followed by coupled transport towards the draw solution. The proposed mechanism is illustrated in Fig. 7. Salting out of the solutes used in this study was shown in Fig. 1 and is known to cause adsorption on less polar surfaces [35–37]. This would cause the solutes to be enriched within the membrane matrix. The solutes however are all highly water soluble, and thus interact strongly with water. Therefore, adsorbed species are assumed to be still available for interactions with water, which can cause desorption and entrainment. Coupled diffusion is a necessary condition for negative rejection: negative rejection cannot be caused by uncoupled diffusive solute transport (disregarding the exception of strong salting in), as this implies "uphill" diffusion. Uphill diffusion however is a well-known phenomenon from coupled diffusion [29]. Coupling between the feed solute and water fluxes is considered, given that these fluxes are directed parallel. This allows the use of Eq. (17).

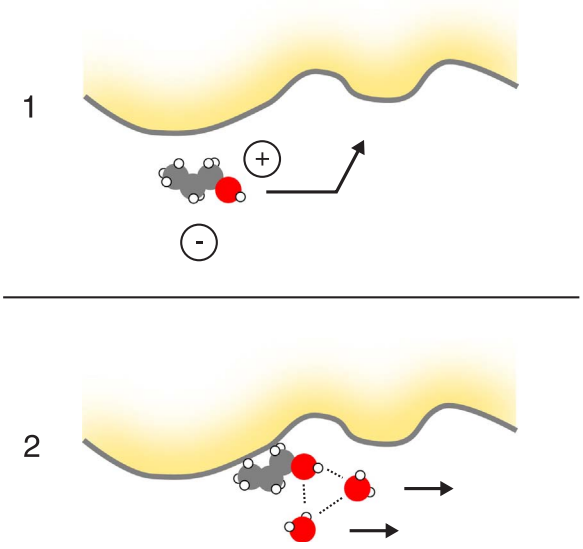

Fig. 7. Schematic of the proposed transport mechanism. In a first step, solutes are subject to adsorption due to salting out, causing enrichment of the solutes within the membrane matrix. In a second step, the highly water-soluble solutes are subject to solute-water interactions, causing coupled diffusion. This results in "uphill" diffusion.

Initial adsorption was modeled as a Langmuir process, assuming a monolayer of adsorbed species on the adsorbent. The assumption in Langmuir theory of a monolayer corresponds well with the view of strong attractive solute-membrane interactions, in which all adsorbed species are contacting the adsorbent. The rate of adsorption J_{ads} is given by:

$$J_{ads} = J_s = k_a c_m (\Sigma_0 - \Sigma_a) \tag{20}$$

in which k_a is a rate constant, Σ_0 and Σ_a are the total and occupied concentration of adsorption sites in the membrane respectively and c_m is the solute concentration at the feed solution - membrane interface. Traditionally, the number of adsorption sites in Langmuir adsorption are expressed as a surface concentration. This can be transformed into a volumetric concentration as well, when the product of the surface concentration and the specific surface area is considered. At steady-state, the adsorption rate matches the solute flux J_s. Rearranging Eq. (20) for Σ_a, the concentration of adsorbed solute, yields:

$$\Sigma_a = \frac{k_a c_m \Sigma_0 - J_s}{k_a c_m} \tag{21}$$

Eq. (17) is now integrated with the following boundary conditions: at the feed side of the membrane, the solute concentration is given by Σ_a, at the draw side, the solute concentration is given by c_p, the latter being desorbed solutes. Integration and substitution of Σ_a with Eq. (21) then yields:

$$J_s = \frac{K_c k_a \Sigma_0 c_m J_w}{k_a c_m \left(1 - (1 - K_c) exp\left(-\frac{J_w K_c L}{K_d D_\infty}\right)\right) + K_c J_w} \tag{22}$$

The hindrance factors K_c and K_d already contain the solute partitioning coefficient ϕ, as ϕ only occurs as a product with the hindrance factors and can thus be omitted [28]. Rearranging for rejection yields:

$$R = 1 - \frac{K_c k_a \Sigma_0}{k_a c_m \left(1 - (1 - K_c) exp\left(-\frac{J_w K_c L}{K_d D_\infty}\right)\right) + K_c J_w} \tag{23}$$

This model will be referred to as *CDL*, as it combines Langmuir adsorption with convection-diffusion-type coupled transport.

Examining the limits of Eq. (23) with respect to k_a yields:

$$\lim_{k_a \to 0} R_{CDL} = 1 \quad \& \quad \lim_{k_a \to \infty} R_{CDL} = 1 - \frac{K_c \Sigma_0}{c_m (1 - (1 - K_c) exp(-\frac{J_w K_c L}{K_d D_\infty}))}$$

which shows that for a very low adsorption rate, rejection equals 1, and that for a very high adsorption rate, the rejection limit resembles Eq. (18). In the latter case, the membrane is saturated with adsorbed solute and J_s is dominated by hindered transport through the membrane. The limits of Eq. (23) for Σ_0 are:

$$\lim_{\Sigma_0 \to 0} R_{CDL} = 1 \quad \& \quad \lim_{\Sigma_0 \to \infty} R_{CDL} = -\infty$$

showing that Σ_0, the total concentration of adsorption sites, is the driving force for solute transport. At very high adsorption capacity, the driving force for adsorption is high as well resulting in strong enrichment of the adsorbing solute compared to the feed solution and very low rejection. In this study, adsorption capacity and the salinity dependence thereof were not independently measured; this will be the subject of future study.

Eqs. (22) and (23) have 5 parameters to be fitted to experimental data (K_c, K_d, L, k_a and Σ_0). When hindered transport theory correlations for K_c and K_d are used [28,32], 4 variables remain: K_c and K_d are then replaced by λ. In this study, no such correlations were used, as it has

been shown recently that such correlations were poor predictors of hindrance factors in dense membranes [38,39]. Independent measurements of adsorption capacity and rate can provide estimates for k_a and Σ_0. If no adsorption measurements are performed, the model can be simplified as follows: in Eq. (20), setting Σ_0 to unity lumps k_a and Σ_0 together as a single variable k_a^* describing the maximal adsorption rate. Likewise, in the Peclet number, L^* can be defined to include K_d: $L^* = L/K_d$. The resulting simplifications yield a model with 3 parameters to be fitted, which was assessed in this study without independently determined adsorption isotherms. One possible source of controversy in this model is that adsorbed solutes were assumed to desorb readily and be available for permeation. In contrast, in the case of very strong adsorption, as was encountered for example by Williams et al. [24], the adsorbed solutes block water permeation and solute permeation is delayed as well. In this study, the membrane's hydraulic permeability was not adversely affected and strong negative rejection was obtained after relatively short filtration tests, showing that the solutes were in fact quite mobile within the membrane.

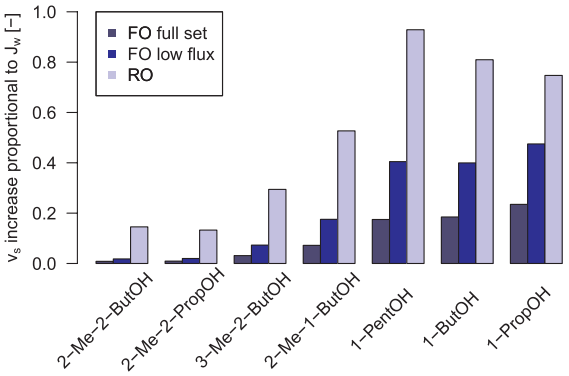

Fig. 9. Increase of solute velocity relative to increasing J_w, normalized for molar volumes, showing the extent of flux coupling between solutes and water. Alcohols are sorted left to right from most to least sterically hindered. Because solute fluxes showed a plateau in FO at increasing J_w, the analysis was also performed on the lower half of the FO dataset with regards to J_w.

5. Coupled fluxes

In the *CDL* model, coupled fluxes of water and the solutes are assumed. Flux coupling can be experimentally shown by plotting J_s as a function of J_w, which yields a positive correlation between J_s and J_w. In the case of uncoupled fluxes, which are assumed in the classical solution-diffusion model, no correlation between J_s and J_w would exist. In order to compare both water and solute fluxes in terms of velocity, the solute fluxes were converted to velocity as follows:

$$v_s = \frac{J_s \bar{v}}{x_f} \tag{24}$$

In Eq. (24), $\bar{v}$ and x_f are the solute's molar volume and feed molar fraction respectively, yielding solute velocity in units of m/s, similar to J_w. The results for the alcohols during both FO (left panel) and RO (right panel) are shown in Fig. 8. The solute velocity is considerably higher than the water flux, which can be explained by the difference in molar volumes between water and the alcohols, the latter's molar volume is roughly 5 times larger compared to water. It can be clearly seen that solute velocity increases with increasing water flux, both during FO and RO. Coupling is clearly stronger for the less sterically hindered alcohols as well. At low fluxes, solute velocity is higher in FO, as was to be expected given the negative rejection. At high fluxes, solute velocity in FO appears to reach a plateau and slightly declines. This could be due to several reasons, which are not mutually exclusive. There could be hindrance between the increasing RSD and alcohol fluxes. Osmotic dehydration of the membrane [40] could also increase steric hindrance between the membrane and permeating solutes. Finally, salting out of the alcohols at increasing salinity (see Fig. 1) increases their activity in the draw solution, decreasing the driving force for membrane permeation. In RO on the other hand, hardly any decline can be seen: solute fluxes increase linearly with water flux.

A clear structure - transport mode relation can be seen as well: the more an alcohol is subject to steric hindrance, the weaker the correlation between water and solute flux. This was quantified using linear regression of solute velocity as a function of the water velocity, taking into account the molar volume difference between the solutes and water. The results are plotted in Fig. 9, where the alcohols are sorted from most to least sterically hindered. Given that in FO the solute velocity as a function of J_w plateaus, regression was done on both the full dataset and on the lower half with regards to J_w, denoted "FO low flux". For the FO tests, it can be seen that the extent of flux coupling between alcohols and water increases as steric hindrance decreases. The most sterically hindered alcohols are barely influenced by J_w, showing that steric hindrance decouples solute transport from water transport. For RO, the pattern is similar but some discrepancies can be noted. Flux coupling is more pronounced in RO compared to FO. This could be due the three reasons given above, and additionally this could also be due to the increased chemical potential of the solutes caused by the hydrostatic pressure applied during RO. Additionally, for the linear alcohols, flux coupling is stronger as the alkyl chain length increases from 1-propanol to 1-pentanol, which is opposite to FO. This can also be

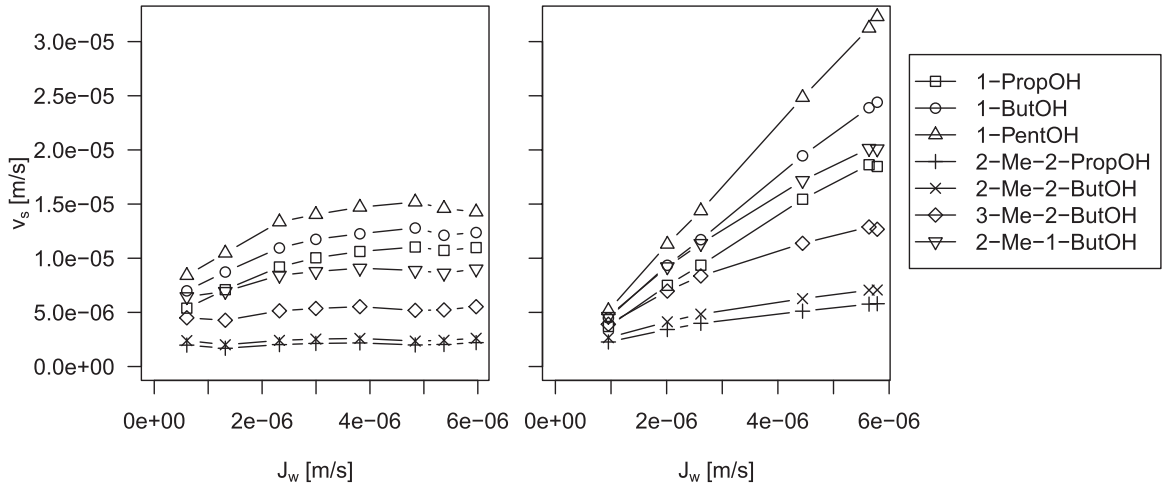

Fig. 8. Solute velocity during FO (left panel) and RO (right panel) filtration. Solute velocity is clearly positively correlated with water flux, indicating flux coupling, for the less sterically hindered alcohols. Flux coupling is weaker for the sterically hindered alcohols.

explained by the effect of hydrostatic pressure on the chemical activity of the solutes: as the alkyl chain length increases, so does the molar volume, and so does the effect of hydrostatic pressure on chemical activity [3,2]. This clearly shows a difference between FO and RO: feed solute activity is not increased during FO operation, but it is during RO operation. If no salting out occurs, it should therefore be possible to attain higher rejections in FO at equal flux and membrane pore size.

Using appropriate models for coupled fluxes, such as Maxwell-Stefan theory, and appropriate models for solute size and steric hindrance, it should be possible to determine the membrane pore size and pore size distribution based on the relation between flux coupling and solute size. In the case of RO, the molar volume influence on chemical activity due to hydrostatic pressure has to be taken into account, as the correlation between J_w and v_s is in part due to hydrostatic pressure and not solely due to the dependence of v_s on J_w. This will be the subject of further study.

6. Novel model performance

6.1. Convergence

The *CDL* model yielded an r^2 of on average 0.991 (min. 0.981, max 0.997); fitting results are shown in Fig. 10. Not all alcohols showed negative rejection, with 2-methyl-2-propanol and 2-methyl-2-butanol showing very similar rejection increasing from 35% to 93% with increasing J_w. Their rejection was however still predicted better by the *CDL* model, as illustrated in Fig. 11: the rejection of 2-methyl-2-propanol is shown, along with model fits by the *CDL*, *CD* and *SK* models (all models allowing flux coupling), with r^2 being 0.982, 0.838 and 0.253 respectively. Both the *CD* and *SK* models overestimated rejection at low flux, but yielded realistic estimates at fluxes in excess of 1 μm/s. The *SK* model yielded a rather poor r^2, however, the *CD* model performed well in the case of 2-methyl-2-propanol: one could be tempted to simply disregard the low rejection at low flux as experimental error. However, when rejection at low flux is reduced further, the *CD* and *SK* models fair much worse. Also shown in Fig. 11 is the rejection of 1-propanol, which varied from −115% to 56% and predictions by the same 3 models, with r^2 being 0.996, 0.187 and 0.245 for the *CDL*, *CD* and *SK* models respectively. Given that the *CD* and *SK* models are not able to predict a rejection pattern such as the one shown by 1-propanol, their predictions are of much poorer quality as well.

6.2. Parameter interpretation

The *CDL* model was solved for 3 lumped, tunable variables: K_c, k_a^* and L^*. Assuming for the alcohols that $K_c \approx 1$ because their size is quite similar to water and because of their high water solubility, $K_c = \phi$, showing that the alcohols are enriched in the membrane phase by a factor of 4–5 compared to the feed solution. The maximal adsorption rate, k_a^*, showed high variability: unsurprisingly, the adsorption rate of alcohols decreased as steric hindrance increased: k_a^* was $3.26 \cdot 10^{-6}$ mol/(m^2s) for 1-propanol, the smallest alcohol and having a linear alkyl chain, while k_a^* was 0.41 and $0.42 \cdot 10^{-6}$ mol/(m^2s) for the most hindered alcohols, 2-methyl-2-propanol and 2-methyl-2-butanol respectively. At $R = 0$, Eq. (23) can be rearranged to give:

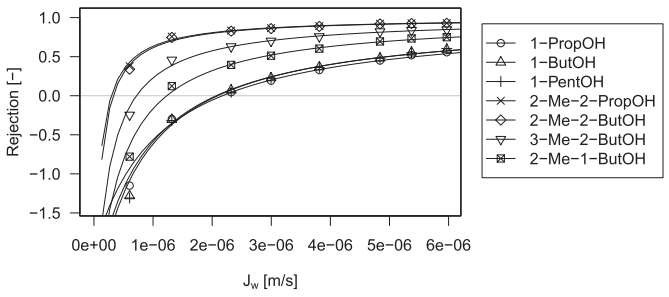

Fig. 10. Experimental rejection and *CDL* model results for alcohol rejection. r^2 was between 0.981 and 0.997 for the different alcohols.

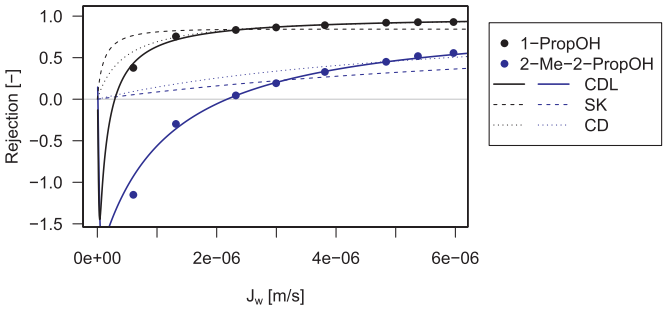

Fig. 11. Experimental rejection of 1-propanol and 2-methyl-2-propanol and predictions by the *CDL*, *CD* and *SK* models.

$$(k_a^*)_{R=0} = \frac{K_c J_w}{K_c - c_m(1 - K_c)exp\left(-\frac{J_w K_c L}{D_\infty}\right)} \quad (25)$$

For large Péclet numbers, Eq. (25) reduces to $k_a^* = J_w$, in which case $R = 0$ is reached once $J_w = k_a^*$. Because the term $-c_m(1 - K_c) > 0$, $R = 0$ is reached at $J_w < k_a^*$ for finite Péclet numbers. k_a^* can thus be regarded as the highest possible flux at which rejection becomes positive.

The calculated Péclet numbers for the alcohols were high, varying from 45 to 450 with increasing flux. This was due to the high values obtained for L^*. The path length term L can be isolated from L^*, by again assuming $\phi \approx K_c$ and $K_d = (0.1 - 1) \cdot 10^{-3}$ [39], then L was on average 8–80 μm. Assuming furthermore an active layer porosity of 0.05 [41,42] which yields a tortuosity of 2 [43], then this would yield an active layer thickness of 100–1000 nm, of which the lower end of the estimate is within the range of expected active layer thickness. Zhang et al. [41] measured the active layer thickness of a CA FO membrane using PALS, finding $l = 852 \pm 530$ nm. Freger [44] studied polyamide active layers of RO and NF membranes, finding thicknesses of 100–300 nm for RO and 14–30 nm for NF membranes. These experimental results show that the calculated CTA membrane thickness is within the expected range, and that K_d is probably close to $1 \cdot 10^{-4}$.

7. Significance of negative rejection and further model refinement

The results presented in this study stem from a somewhat more fundamental study of a peculiar mass transport phenomenon in FO. Salting-out and subsequent preferential transport of organic compounds could however have a significant impact in FO, as FO would typically be applied on feed streams having high organics concentrations. Such feeds are for instance waste water, waste water treatment sludge, fresh or spent fermentation broths and liquid foods. Under most circumstances, preferential transport of organics would be unwanted: when FO is applied to recycle water from waste water or to dehydrate liquid foods, the FO permeate should ideally not contain any feed solutes. Preferential solute transport could be beneficial as well if for instance in-line extraction of products from a (bio-)reactor is sought. The FO tests presented in this study were all performed using feed solutions consisting of deionized water spiked with the 7 alcohols, and using a virgin membrane sample. In full-scale FO applications, this will obviously not be the case: in all likelihood, FO feeds will be complex mixtures of many different organic and inorganic solutes and colloids. Suspended and colloidal matter could compete with the membrane for adsorption sites of small organic compounds, thereby diminishing the amount of organics adsorbing onto the membrane. However, the salinity of the draw solution is higher compared to the feed solution and does not contain colloidal or suspended matter. Feed solutes permeating through the active layer could therefore still be subject to

salting out and adsorption onto the membrane, despite the presence of competing organic particles in the feed solution.

The model presented in this study relies on adsorption, in which equilibrium adsorbate concentrations are dependent on both adsorbent and adsorbate concentrations. Alcohols were dosed at 100 mg/L, many orders of magnitude higher than concentrations of organic micropollutants (OMPs) in waste water, which are found in concentrations up to 1 μg/L [45]. However, the influence of salinity on OMP phase distribution behavior at environmentally relevant concentrations has been shown experimentally [36,37,46]. Further tests at much lower solute concentrations are needed to assess the relevance of this model for OMPs. It should be noted however that with increasing steric hindrance, flux coupling between water and feed solutes becomes progressively weaker, as was shown in Section 5, with flux coupling being a necessary condition for negative rejection following adsorption. This casts doubt on the relevance of this model for relatively large molecules such as OMPs, whose size approaches the membrane pore size: OMPs, such as pharmaceuticals, pesticides or personal care products, are considerably larger than the alcohols used in this study.

Further model refinement is possible: in the current model, both adsorption capacity and solute diffusivity are assumed to be constant with respect to salinity. The assumption of constant diffusivity is valid when the solute chemical potential gradient equals a concentration gradient. This is commonly the case for dilute solutions, in which the solute's activity coefficient approaches unity at infinite dilution. However, in the case of salting out, this is obviously not the case: salting out is, by definition, an increased chemical activity of the solute due to a change in the solvent composition. Likewise, a constant adsorption capacity with respect to salinity is unlikely: earlier studies on adsorption of OMPs on natural organic particles in saline environments show increasing adsorption capacity at increasing salinity [36,37]. The new model however yields an excellent fit. This is likely due to counteracting effects of adsorption and feed solute chemical activity. At increasing salinity, an increasing adsorption capacity would cause stronger negative rejection, while an increasing feed solute chemical activity in the saline environment of the draw solution would create a driving force for back-diffusion of the feed solute from the draw to the feed solution, causing increasing rejection.

8. Conclusions

Negative rejection of 7 alcohols, being uncharged, hydrophilic solutes, was encountered during FO. The rejection was strongly negative for most alcohols at lower water fluxes, becoming positive at increasing fluxes. Curiously, this pattern could not be reproduced using popular transport models: models were reviewed in this study and it was shown that they either could not explain negative rejection, or could not reproduce the same rejection pattern. It was also shown that negative rejection is only possible when coupled transport is occurring: negative rejection, being enrichment of a solute in the permeate stream, requires “uphill” diffusion. Consequently, a mechanistic model was developed, consisting of enrichment of the solutes within the membrane matrix due to adsorption followed by coupled transport. Adsorption of the solutes was due to salting out of the alcohols, which has been described in earlier studies [47,48], and was experimentally verified from headspace-GC-MS measurements in this study as well. Excellent agreement between the experimental data and newly developed model was obtained.

RO filtration was performed as well, using the same solutes and membrane, which was operated at similar fluxes. In both FO and RO, the alcohols displayed a clear structure-permeability relation. During RO however, no negative rejection was obtained. It was also shown that in RO, alcohol fluxes correlated stronger to the water flux, likely due to stronger flux coupling combined with the solutes' increased activity due to hydrostatic pressure. Because the latter effect is absent in FO, it should be possible to obtain higher solute rejection in FO, if of course no adsorption occurs.

The cause of the initial alcohol adsorption was shown to be salting out. In the context of membrane filtration, the rate of adsorption was shown to have a large impact on rejection: branched, sterically hindered alcohols showed less negative rejection compared to straight chain alcohols, or even showed no negative rejection at all. Given that more sterically hindered molecules permeate slower, long-term tests are needed to assess time-dependence of adsorption and permeation of such compounds. This is true for the alcohols used in this study, but is also relevant for other OMPs. Salting out could have significant consequences in FO: FO operation depends on a highly concentrated draw solution, thus salting effects on permeating feed solutes are to be expected, and can be both beneficial or detrimental, depending on the application.

Appendix A. Supplementary data

Supplementary data associated with this article can be found in the online version at http://dx.doi.org/10.1016/j.memsci.2017.11.002.

References

[1] D. Bhanushali, S. Kloos, D. Bhattacharyya, Solute transport in solvent-resistant nanofiltration membranes for non-aqueous systems experimental results and the role of solute - solvent coupling, J. Membr. Sci. 208 (2002) 34–359 PiiS0376-7388(02)00315-0..

[2] D. Paul, Reformulation of the solution-diffusion theory of reverse osmosis, J. Membr. Sci. 241 (2) (2004) 371–386, http://dx.doi.org/10.1016/j.memsci.2004.05.026.

[3] J.G. Wijmans, R.W. Baker, The solution-diffusion model: a review, J. Membr. Sci. 107 (1–2) (1995) 1–21, http://dx.doi.org/10.1016/0376-7388(95)00102-I.

[4] D. Bhanushali, S. Kloos, C. Kurth, D. Bhattacharyya, Performance of solvent-resistant membranes for non-aqueous systems: solvent permeation results and modeling, J. Membr. Sci. 189 (1) (2001) 1–21, http://dx.doi.org/10.1016/S0376-7388(01)00356-8.

[5] P. Vandezande, L.E.M. Gevers, I.F.J. Vankelecom, Solvent resistant nanofiltration: separating on a molecular level, Chem. Soc. Rev. 37 (2) (2008) 365–405, http://dx.doi.org/10.1039/B610848M.

[6] S. Postel, G. Spalding, M. Chirnside, M. Wessling, On negative retentions in organic solvent nanofiltration, J. Membr. Sci. 447 (2013) 57–65, http://dx.doi.org/10.1016/j.memsci.2013.06.009.

[7] A. Malakhov, A. Volkov, Application of coupled solution-diffusion model in organic solvent nanofiltration: positive and negative rejection of solutes, Sep. Sci. Technol. 6395 (May) (2015) 2198–2210, http://dx.doi.org/10.1080/01496395.2015.1031403.

[8] A.E. Yaroshchuk, Negative rejection of ions in pressure-driven membrane processes, Adv. Colloid Interface Sci. 139 (1–2) (2008) 150–173, http://dx.doi.org/10.1016/j.cis.2008.01.004.

[9] M. Perry, C. Linder, Intermediate reverse osmosis ultrafiltration (RO UF) membranes for concentration and desalting of low molecular weight organic solutes, Desalination 71 (3) (1989) 233–245, http://dx.doi.org/10.1016/0011-9164(89)85026-X.

[10] H.K. Lonsdale, U. Merten, M. Tagami, Phenol transport in cellulose acetate membranes, J. Appl. Polym. Sci. 11 (9) (1967) 1807–1820, http://dx.doi.org/10.1002/app.1967.070110917.

[11] T. Matsuura, S. Sourirajan, Reverse osmosis separation of phenols in aqueous solutions using porous cellulose acetate membranes, J. Appl. Polym. Sci. 16 (10) (1972) 2531–2554, http://dx.doi.org/10.1002/app.1972.070161008.

[12] H. Burghoff, K. Lee, W. Pusch, Characterisation of transport across cellulose-acetate membranes in the presence of strong solute-membrane interactions, J. Appl. Polym. Sci. 25 (1980) 323.

[13] S. Mandale, M. Jones, Membrane transport theory and the interactions between electrolytes and non-electrolytes, Desalination 252 (1–3) (2010) 17–26, http://dx.doi.org/10.1016/j.desal.2009.11.007.

[14] C.J. van Oss, Interfacial Forces in Aqueous Media, 2nd edition, Taylor and Francis Group, LLC, 2006.

[15] F.A. Long, W.F. McDevit, Activity coefficients of nonelectrolyte solutes in aqueous salt solutions, Chem. Rev. 51 (1) (1952) 119–169.

[16] L. Hao, D.G. Leaist, Binary mutual diffusion coefficients of aqueous alcohols. Methanol to 1-heptanol, J. Chem. Eng. Data 41 (1996) 210–213, http://dx.doi.org/10.1021/je950222q.

[17] T. Funazukuri, Infinite dilution binary diffusion coefficients of C 5 -monoalcohols in the temperature range from 273.2 K to 353.2 K at 0.1 MPa, J. Chem. Eng. Data 44 (1999) 73–76.

[18] M. Mulder, Basic Principles of Membrane Technology, 2nd edition, Springer, 1996.

[19] G. Schock, A. Miquel, Mass transfer and pressure loss in spiral wound modules, Desalination 64 (1987) 339–352.

[20] C.P. Koutsou, S.G. Yiantsios, a.J. Karabelas, a.J. Karabelas, A numerical and experimental study of mass transfer in spacer-filled channels: effects of spacer

geometrical characteristics and Schmidt number, J. Membr. Sci. 326 (1) (2009) 234–251, http://dx.doi.org/10.1016/j.memsci.2008.10.007.
[21] A. Wahab Mohammad, Simple mass transfer experiment using NF membranes, Chem. Eng. Educ. 34 (3) (2000) 264–267.
[22] R Core Team, R: A Language and Environment for Statistical Computing, 2016.URL ⟨https://www.r-project.org/⟩.
[23] B. Van Der Bruggen, J. Schaep, D. Wilms, C. Vandecasteele, Influence of molecular size, polarity and charge on the retention of organic molecules by nanofiltration, J. Membr. Sci. 156 (1999) 29–41.
[24] M.E. Williams, J.A. Hestekin, C.N. Smothers, D. Bhattacharyya, Separation of organic pollutants by reverse osmosis and nanofiltration membranes: mathematical models and experimental verification, Ind. Eng. Chem. Res. 38 (September) (1999) 3683–3695, http://dx.doi.org/10.1021/ie9901401.
[25] K.S. Spiegler, O. Kedem, Thermodynamics of hyperfiltration (reverse osmosis): criteria for efficient membranes, Desalination 1 (4) (1966) 311–326, http://dx.doi.org/10.1016/S0011-9164(00)80018-1.
[26] W.R. Bowen, a.W. Mohammad, N. Hilal, a.W. Mohammad, N. Hilal, Characterisation of nanofiltration membranes for predictive purposes - use of salts, uncharged solutes and atomic force microscopy, Journal of Membrane Science, 126.
[27] S. Bason, O. Kedem, V. Freger, Determination of concentration-dependent transport coefficients in nanofiltration: experimental evaluation of coefficients, J. Membr. Sci. 326 (1) (2009) 197–204, http://dx.doi.org/10.1016/j.memsci.2008.09.054.
[28] P. Dechadilok, W.M. Deen, Hindrance factors for diffusion and convection in pores, Ind. Eng. Chem. Res. 45 (21) (2006) 6953–6959, http://dx.doi.org/10.1021/ie051387n.
[29] R. Krishna, J. Wesselingh, The Maxwell-Stefan approach to mass transfer, Chem. Eng. Sci. 52 (6) (1997) 861–911, http://dx.doi.org/10.1016/S0009-2509(96)00458-7.
[30] P.J.A.M. Kerkhof, M.A.M. Geboers, Analysis and extension of the theory of multicomponent fluid diffusion, Chem. Eng. Sci. 60 (12) (2005) 3129–3167, http://dx.doi.org/10.1016/j.ces.2004.12.042.
[31] B. Ghanbarian, A.G. Hunt, R.P. Ewing, M. Sahimi, Tortuosity in porous media: a critical review, Soil Sci. Soc. Am. J. 77 (5) (2013) 1461–1477, http://dx.doi.org/10.2136/sssaj2012.0435.
[32] V. Silva, P. Prádanos, L. Palacio, A. Hernández, Alternative pore hindrance factors: what one should be used for nanofiltration modelization? Desalination 245 (1–3) (2009) 606–613, http://dx.doi.org/10.1016/j.desal.2009.02.026.
[33] A.R.D. Verliefde, E.R. Cornelissen, S.G.J. Heijman, E.M.V. Hoek, G.L. Amy, B. Van der Bruggen, J.C. Van Dijkt, Influence of solute-membrane affinity on rejection of uncharged organic solutes by nanofiltration membranes, Environ. Sci. Technol. 43 (7) (2009) 2400–2406.
[34] J. Wang, Y. Mo, S. Mahendra, E.M. Hoek, Effects of water chemistry on structure and performance of polyamide composite membranes, J. Membr. Sci. 452 (2014) 415–425, http://dx.doi.org/10.1016/j.memsci.2013.09.022.
[35] R. Aveyard, M. Saleem, Salt effects on adsorbed nonelectrolytes, Can. J. Chem. 55 (1977) 4018–4027.
[36] A. Turner, M.C. Rawling, The influence of salting out on the sorption of neutral organic compounds in estuaries, Water Res. 35 (18) (2001) 4379–4389.
[37] A. Turner, Salting out of chemicals in estuaries: implications for contaminant partitioning and modelling, Sci. Total Environ. 314–316 (2003) 599–612, http://dx.doi.org/10.1016/S0048-9697(03)00076-7.
[38] E. Dražević, K. Košutić, V. Kolev, V. Freger, Does hindered transport theory apply to desalination membranes? Environ. Sci. Technol. 48 (19) (2014) 11471–11478, http://dx.doi.org/10.1021/es502085p.
[39] D.S. Dlamini, S. Levchenko, M. Bass, B.B. Mamba, E.M.V. Hoek, J.M. Thwala, V. Freger, Solute hindrance in non-porous membranes: an ATR-FTIR study, Desalination 368 (2015) 60–68, http://dx.doi.org/10.1016/j.desal.2015.03.009.
[40] A. D'Haese, M.M. Motsa, P. Van der Meeren, A.R. Verliefde, A refined draw solute flux model in forward osmosis: theoretical considerations and experimental validation, J. Membr. Sci. 522 (2017) (2017) 316–331, http://dx.doi.org/10.1016/j.memsci.2016.08.053.
[41] S. Zhang, K.Y. Wang, T.-S. Chung, H. Chen, Y.C. Jean, G. Amy, Well-constructed cellulose acetate membranes for forward osmosis: minimized internal concentration polarization with an ultra-thin selective layer, J. Membr. Sci. 360 (1–2) (2010) 522–535, http://dx.doi.org/10.1016/j.memsci.2010.05.056.
[42] R.C. Ong, T.S. Chung, B.J. Helmer, J.S. De Wit, Characteristics of water and salt transport, free volume and their relationship with the functional groups of novel cellulose esters, Polym. (U.K.) 54 (17) (2013) 4560–4569, http://dx.doi.org/10.1016/j.polymer.2013.06.043.
[43] L. Shen, Z. Chen, Critical review of the impact of tortuosity on diffusion, Chem. Eng. Sci. 62 (14) (2007) 3748–3755, http://dx.doi.org/10.1016/j.ces.2007.03.041.
[44] V. Freger, Swelling and morphology of the skin layer of polyamide composite membranes: an atomic force microscopy study, Environ. Sci. Technol. 38 (11) (2004) 3168–3175.
[45] T.A. Ternes, Occurrence of drugs in german sewage treatment plants and rivers, Water research, 32 (11).
[46] Y. Chen, J.L. Zhou, L. Cheng, Y.Y. Zheng, J. Xu, Sediment and salinity effects on the bioaccumulation of sulfamethoxazole in zebrafish (Danio rerio), Chemosphere 180 (2017) 467–475, http://dx.doi.org/10.1016/j.chemosphere.2017.04.055.
[47] R. Aveyard, R. Heselden, Salting out of alkanols by inorganic electrolytes.pdf, J. Chem. Soc.: Faraday Trans. 1 (2) (1975) 312–321.
[48] R. De Santis, L. Marrelli, P.N. Muscetta, Liquid-liquid equilibria in water-aliphatic alcohol systems in the presence of sodium chloride, Chem. Eng. J. 11 (3) (1976) 207–214, http://dx.doi.org/10.1016/0300-9467(76)80042-1.